electronics

MDPI

Article

Analysis of Minimal Channel Electroencephalography for Wearable Brain–Computer Interface

Arpa Suwannarat [1], Setha Pan-ngum [2,*] and Pasin Israsena [1]

[1] National Electronics and Computer Technology Center, National Science and Technology Development Agency (NSTDA), Pathum Thani 12120, Thailand; arpa.suw@nectec.or.th (A.S.); pasin.israsena@nectec.or.th (P.I.)
[2] Department of Computer Engineering, Faculty of Engineering, Chulalongkorn University, Bangkok 10330, Thailand
* Correspondence: setha.p@chula.ac.th

Abstract: Electroencephalography (EEG)-based brain—computer interface (BCI) is a non-invasive technology with potential in various healthcare applications, including stroke rehabilitation and neuro-feedback training. These applications typically require multi-channel EEG. However, setting up a multi-channel EEG headset is time-consuming, potentially resulting in patient reluctance to use the system despite its potential benefits. Therefore, we investigated the appropriate number of electrodes required for a successful BCI application in wearable devices using various numbers of EEG channels. EEG multi-frequency features were extracted using the "filter bank" feature extraction technique. A support vector machine (SVM) was used to classify a left/right-hand opening/closing motor imagery (MI) task. Nine electrodes around the center of the scalp (F3, Fz, F4, C3, Cz, C4, P3, Pz, and P4) provided high classification accuracy with a moderate setup time; hence, this system was selected as the minimal number of required channels. Spherical spline interpolation (SSI) was also applied to investigate the feasibility of generating EEG signals from limited channels on an EEG headset. We found classification accuracies of interpolated groups only, and combined interpolated and collected groups were significantly lower than the measured groups. The results indicate that SSI may not provide additional EEG data to improve classification accuracy of the collected minimal channels. The conclusion is that other techniques could be explored or a sufficient number of EEG channels must be collected without relying on generated data. Our proposed method, which uses a filter bank feature, session-dependent training, and the exploration of many groups of EEG channels, offers the possibility of developing a successful BCI application using minimal channels on an EEG device.

Keywords: brain—computer interface (BCI); motor imagery (MI); common spatial pattern (CSP); rehabilitation technology

check for updates

Citation: Suwannarat, A.; Pan-ngum, S.; Israsena, P. Analysis of Minimal Channel Electroencephalography for Wearable Brain–Computer Interface. *Electronics* **2024**, *13*, 565. https://doi.org/10.3390/electronics13030565

Academic Editor: Juan M. Corchado

Received: 14 December 2023
Revised: 18 January 2024
Accepted: 21 January 2024
Published: 30 January 2024

Copyright: © 2024 by the authors. Licensee MDPI, Basel, Switzerland. This article is an open access article distributed under the terms and conditions of the Creative Commons Attribution (CC BY) license (https://creativecommons.org/licenses/by/4.0/).

1. Introduction

Wearable technology is increasingly being adopted in healthcare. For example, in cardiology, diagnostic information can be acquired using wearable devices [1–4]. Further, epilepsy and sleep disorders can be detected via wearable technology [5–8]. Increasing health awareness among the general public has also popularized the use of smart devices, such as fitness trackers that connect to mobile phones. Furthermore, for research purposes, wearable devices are a practical means for collecting useful information during clinical trials, such as an individual's length of sleep and heart rate. These applications demonstrate that wearable technology has a promising future in healthcare.

Brain—computer interface (BCI) is an emerging technology that allows for humans to use brain signals to communicate with external devices [9,10]. Conceptually, BCI involves analyzing brain signals and translating them into commands. These commands can then be

used to control external devices. Of all the available BCI modalities, electroencephalography (EEG) is among the most widely used. Not only is EEG-based BCI a non-invasive method, but it is also relatively low-cost and easy to install.

BCI can be applied to monitoring, medical treatment, and rehabilitation [11–14]. For example, stroke is a major cause of disability and death worldwide, and stroke rehabilitation has thus far been proven as a useful and interesting application for EEG-based BCI [12–17]. In EEG-based BCI stroke rehabilitation, detecting motor imagery (MI) is a major study area. A key challenge being studied is how to maximize the capacity to detect MI [18]. MI is the result of movements or imaging of motor action, leading to changes in brain rhythms known as sensorimotor rhythms (SMRs). SMRs are brain rhythms in the alpha/mu band (8–13 Hz) and beta band (13–30 Hz) [9,10]. During MI tasks, phenomena, referred to as event-related desynchronization (ERD) and event-related synchronization (ERS), occur in the brain motor-cortex area [9,10,19]. ERD involves reduced mu rhythm across the sensorimotor cortex during movement preparation and actual movement. Similarly, ERS involves an increase in the mu rhythm across the sensorimotor cortex during the post-movement period [9,10,20]. In addition to this, power suppression (power desynchronization) can be found in the lower theta and alpha bands, which is believed to be associated with attention [21,22]. Desynchronization is also observed in the upper alpha band, which reflects the semantic memory process [21,23]. Beta synchronization and gamma oscillations are also present. Beta synchronization is a post-movement phenomenon and reaches its maximum following movement. Finally, gamma oscillations occur during movement execution and reach their maximum shortly before movement onset [19].

MI can be elicited by imagining one's body movement from a third-person or first-person perspective [24,25]. The latter may induce kinesthetic feeling in body parts during the imagined movement [26]. This method is called kinesthetic motor imagery (KMI). In addition to actively imagining movement, MI can also be elicited by watching motor action [27,28]. This action observation can be performed via a monitor or virtual reality (VR) headset [29,30]. Combining VR-based action observation with KMI was reported to improve motor imagery performance by enhancing brain rhythmic patterns and providing better task differentiation [31].

The most basic MI detection performance measurement is classification accuracy [32]. This metric is generally computed offline using a cross-validation strategy [32,33]. To achieve the goal of high classification accuracy of MI detection, various channel selection/feature extraction algorithms have been proposed, particularly the common spatial pattern (CSP) [34,35]. The CSP is arguably a state-of-the-art algorithm, which has low computational costs and is simple to implement. It is a highly successful algorithm suitable for classifying two MI classes [32,33]. The CSP algorithm is a feature extraction algorithm that attempts to construct an optimal filter that can maximize variance in one class of EEG signals and minimize variance of another [32,33]. Many algorithms derived from CSP have also been proposed [36–40]. The CSP and its derived algorithms are considered methods of channel selection as they incorporate feature selection in their algorithms. Although low computation cost is a benefit of these algorithms, they still require a large number of electrodes.

Linear classifiers are more widely used than non-linear classifiers in MI-based BCI [32,33]. Linear classifiers have fewer parameters than non-linear classifiers and, hence, are less prone to overfitting. Moreover, linear classifiers require less computation time and consume less memory compared with non-linear classifiers [41–43], enabling more suitable real-time applications [41,44,45].

Leveraging EEG-based BCI with a smaller number of channels is supported by several studies [46–49]. EEG-based BCI with a lower number of channels has received considerable attention to date. According to a previous study [50], multi-channel headsets generally require lengthy setup times. A setup time of more than 30 min tends to make participants uncomfortable and unwilling to cooperate in experiments. Headsets using wet electrodes can also make participants physically and emotionally irritated. Using a lower number of

channels not only makes the system more user-friendly but also helps reduce electrode preparation time and achieve good reliability. Moreover, a lower number of channels may reduce the risk of overfitting [51,52].

Channel selection is an interesting topic for minimal channel system development. Various EEG channel selection methods along with their applications, such as seizure detection, motor imagery classification, emotion classification, etc., were reviewed by [53]. Notable techniques are filtering techniques, which include CSP filter, wrapper, embedded, and hybrid techniques. The filtering techniques have low computational costs, so they have high speed, have independence from the classifier, and are simple to implement. The wrapper techniques are more computationally expensive than the filtering techniques and are also prone to overfitting. The embedded techniques are computationally less expensive and less prone to overfitting than the wrapper techniques. The hybrid techniques take advantage of both filtering techniques and wrapper techniques by combining them [50].

Most studies have used conventional BCIs [18,54,55], which have 32 or more channels. However, some studies have used EEG headsets with fewer electrodes. For example, studies by Ang and colleagues used an EEG headset with a minimum of 27 electrodes to detect MI [16,32,38,56]. Therefore, it is interesting to explore an EEG-based MI training system with fewer channels not only for practical purposes but also for potential use in external applications, such as mobile rehabilitation or assistive robotics when combined with an exoskeleton [57].

Interpolation enables EEG signal construction from failed electrodes (or an electrode with poor signal quality) by using information from nearby electrodes. Typically, electrodes with poor signal quality are identified at an early stage of pre-processing. This process significantly affects the efficiency of EEG-based BCI systems. Poor electrode signals are clearly flatter or noisier compared with the signals from surrounding electrodes [58]. Spherical spline interpolation (SSI) is the most widely used interpolation algorithm [59] and is included in many MATLAB toolboxes, such as EEGLAB and ERPLAB [60,61]. Although it is not possible to fully recover a lost EEG signal, interpolation techniques can reconstruct EEG signals using information from surrounding electrodes. Reconstructed signals can then provide information to increase classification accuracy; hence, EEG signal interpolation could be advantageous in this study.

In summary, this study offers insight into the trade-offs between channel number and system performance. EEG signals are characterized by a random, non-stationary, low signal-to-noise ratio and are extremely susceptible to interference. Not every data channel provides useful information, and channel selection helps eliminate irrelevant or redundant EEG channels and improve decoding rates of the BCI system. In particular, we studied the effects using a small number of channels, which is a key criterion for successful wearable devices. Generating additional EEG data using an interpolation technique to enhance classification performance was also assessed. Together with relatively short setup times due to a small number of verified EEG channels, our work contributes to BCI application in MI training and exercise.

2. Materials and Methods

The results from our dataset are presented as classification accuracies for classifying left- and right-hand movement during the opening/closing task. The classification parameters were the session-dependent experiment with varying electrode numbers using the FB feature. The statistical analysis involved a paired *t*-test and ANOVA with Bonferroni correction performed using IBM SPSS Statistics (Version 25) (IBM Corp., New York, NY, USA). The significance level was set at 5% or a *p*-value of 0.05 for all statistical analyses.

2.1. Participants

Eleven healthy male participants aged 18 to 32 years and recruited from Chulalongkorn University, Bangkok, Thailand participated in this study. This study was part of a collaborative research project between the Faculty of Medicine, Chulalongkorn University, Bangkok,

Thailand and the National Electronics and Computer Technology Center, Pathum Thani, Thailand. This study was approved by the institutional review board of the Faculty of Medicine, Chulalongkorn University. All participants provided written informed consent prior to taking part in this study.

All participants were new to BCI usage. Healthy participants were recruited because ERD and ERS can be observed in healthy individuals as well as stroke patients. Furthermore, ERD and ERS responses are more pronounced in healthy individuals compared with other groups, such as active aging [19]. Studies show that ERD and ERS classification performances in both stroke patients and healthy individuals are similar [18,62,63]. A study by Ang and colleagues also found that neurological damage to stroke patients does not significantly affect their capacity to undergo MI–BCI [18].

2.2. EEG Data Acquisition

EEG signals were obtained using a dry EEG electrode g.Nautilus headset with 16 channels (g.tec medical engineering GmbH, Schiedlberg, Austria). EEG signals were recorded from 11 electrodes (F3, FZ, F4, T7, C3, CZ, C4, P3, PZ, and P4) and arranged according to the international 10/20 system, as shown in Figure 1 [64]. These eleven positions were chosen because they cover the C3 to C4 positions along the center of the scalp where hand and arm movements are detected with electrodes [35]. Reference and ground electrodes were placed behind both ears (mastoid). The recorded EEG data were processed using MATLAB (The Mathworks Inc., Natick, MA, USA).

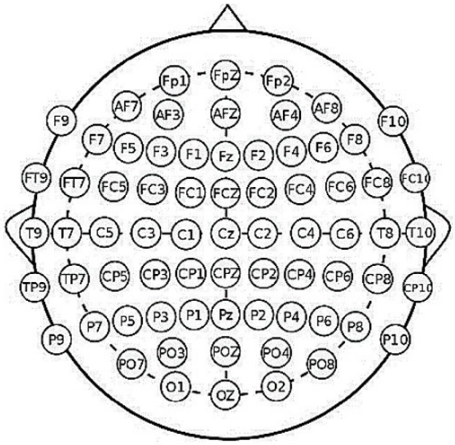


Figure 1. The international 10/20 system [64].

2.3. EEG Signal Processing

The electrodes were grouped as shown in Figure 2. The blue dots indicate the chosen electrodes for each group:

A group of two electrodes, comprising C3 and C4.
A group of three electrodes, comprising C3, Cz, and C4.
A group of five electrodes, comprising T7, C3, Cz, C4, and T8—this group was referred to as 5A.
A group of five electrodes, comprising Fz, C3, Cz, C4, and PZ—this group was referred to as 5B.
A group of nine electrodes, comprising F3, Fz, F4, C3, Cz, C4, P3, Pz, and P4.
A group of eleven electrodes, comprising F3, Fz, F4, T7, C3, Cz, C4, T8, P3, Pz, and P4.

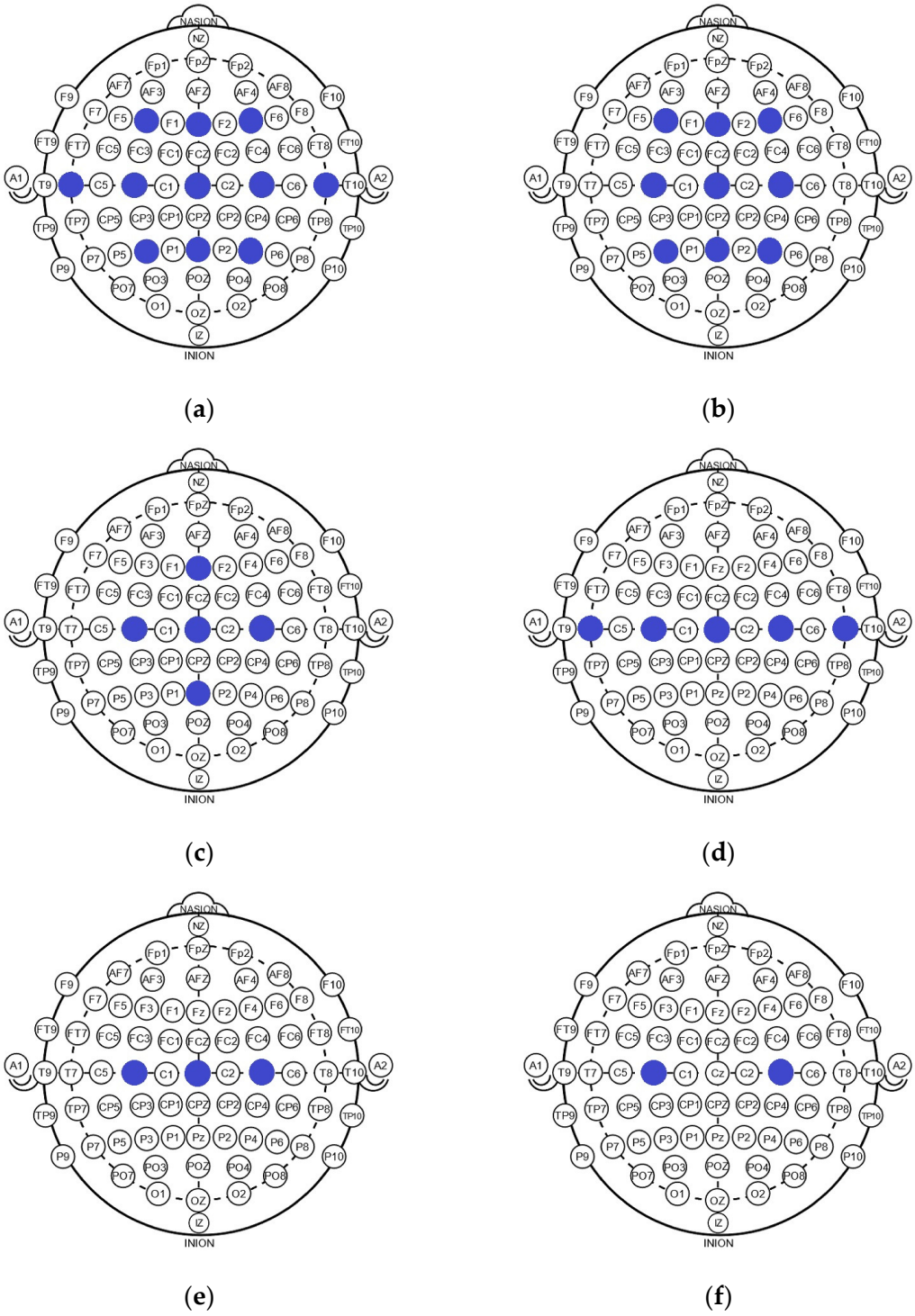


Figure 2. Groups of electrodes used for experiments. (**a**) Group of eleven; (**b**) Group of nine; (**c**) Group of 5B; (**d**) Group of 5A; (**e**) Group of three; (**f**) Group of two.

The EEG data were extracted at 3 and 4 s for each trial, as shown in Figure 3, and the signals were digitally sampled at 250 Hz and band-passed from 8 to 30 Hz, which is the SMRs rhythm, using a fifth-order Butterworth filter.



Figure 3. Timeline of each experimental trial.

We assessed conventional CSP and filter bank (FB) efficiency according to a previous study [51]. The FB band-passed and filtered the collected EEG data into 8–12, 12–16, 16–20, 20–24, 24–28, and 26–30 Hz frequency bands. The results show that the FB features provided significantly higher classification accuracy than conventional CSP with *p*-values less than 0.001 [50]. Several studies suggest that the classification accuracy of each EEG data collection session should be considered separately [65–67]. This paradigm is referred to as "session-dependent." Therefore, the FB feature and session-dependent paradigm were chosen for the present study.

2.4. Classifiers

Lotte et al. [32,33] claimed that linear discriminant analysis (LDA) and support vector machine (SVM) remain the most popular types of classifiers for EEG-based BCI, particularly for online and real-time BCIs, during the past ten years [30]. LDA and SVM are linear classifiers that generally contain fewer parameters than non-linear classifiers. Hence, they require less computational time and memory, making them suitable for real-time applications. According to these studies [34,35], CSP output is the variance of both signal classes, which are close to normal distribution [16]. Therefore, the feature vectors from calibration can be used to estimate parameters for linear classifiers. Accordingly, combining CSP with linear classifiers provides good classification accuracy when detecting MI. SVM, however, is suitable for classifying high-variance signals, such as EEG, due to its desirable characteristics of noise tolerance and high-dimensionality robustness [32,33,41,42].

In the present study, SVM was chosen due to its noise tolerance and high-dimensionality robustness [33]. As there were eight sessions per participant, we performed classification using an eight-fold cross-validation method. We performed EEG data processing offline. First, the extracted EEG data were bandpass filtered. The FB feature was then applied to the filtered data. The outputs for the feature extraction algorithm were then categorized as feature vectors. Finally, the SVM classification models were trained using feature vectors, session-by-session, for each participant and each electrode group.

2.5. Spherical Spline Interpolation (SSI)

Spline interpolation is used for data fitting and estimating the missing data using existing data [68]. Spline comes from a special type of piecewise polynomial. Since the head is modeled as a sphere, Perrin et al. [69] proposed the spherical spline interpolation (SSI) as an interpolation method.

Spherical splines estimate the potential $V(r_i)$ at any point r_i on the surface of the sphere by

$$V(r_i) = c_0 + \sum_{j=1}^{N} c_i g_m(\cos(r_i, r_j)) \quad (1)$$

The cosine function is to compute the angle between electrode r_i and r_j, where located by their spherical coordinates. The function $g_m(\cdot)$ of order m is given by

$$g_m(x) = \frac{1}{4\pi} \sum_{n=1}^{\infty} \frac{2n+1}{(n(n+1))^m} P_n(x) \quad (2)$$

where $P_n(x)$ are Legendre polynomials of order n. Legendre polynomials are applied to estimate the electrical potential at a scalp position. The electrical potential expansion characteristics along the scalp can be represented by the Legendre polynomial. This is because the polynomial parameters vary according to the angles between the scalp locations [68]. To interpolate $V(r_i)$, according to Equation (1), the N + 1 spline coefficients c_i are the constant that must be computed. Once the coefficients are estimated, the average of the referenced potentials is computed. Finally, interpolated data are estimated using both the spline coefficients and the average of the referenced potentials [59].

For interpolation experiments, SSI is an interpolation technique that requires simpler mathematical computation, which is the main advantage of this technique. Therefore, in the present study, the SSI interpolation algorithm was applied to investigate the possibility of applying interpolation and further reducing the number of EEG channels.

2.6. Experimental Paradigm

During the trials, the participants sat comfortably facing a computer screen and were instructed to perform MI tasks using their left and then right hand. The distance between the participants and computer screen was approximately 1 m. The MI task involved hand opening/closing, as shown in Figure 4. Hand opening/closing is not only a major MI task, but the movement is also a basic movement used in stroke rehabilitation, which involves a basic, grasping object motion [70].

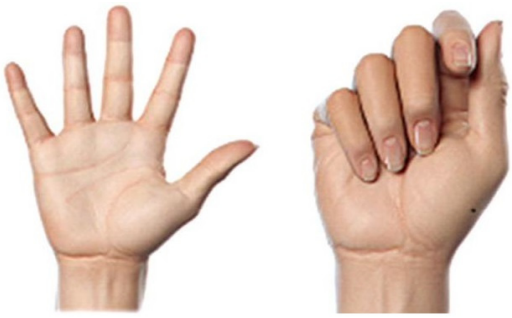


Figure 4. Hand opening and closing task.

All participants completed eight sessions. Each session comprised eight runs of EEG data collection. The participants performed right-hand MI for the first four runs and left-hand MI for the remaining four runs with each run comprising 20 trials. Each trial lasted 7 s, as outlined in Figure 1, and each session lasted approximately 1 h, including setup time. Each participant took part in two experimental sessions per week, and the experiment was completed in four weeks. To instruct the participants to perform MI according to the trial timeline, the screen displayed an image of the required hand movement, as shown in Figure 5.

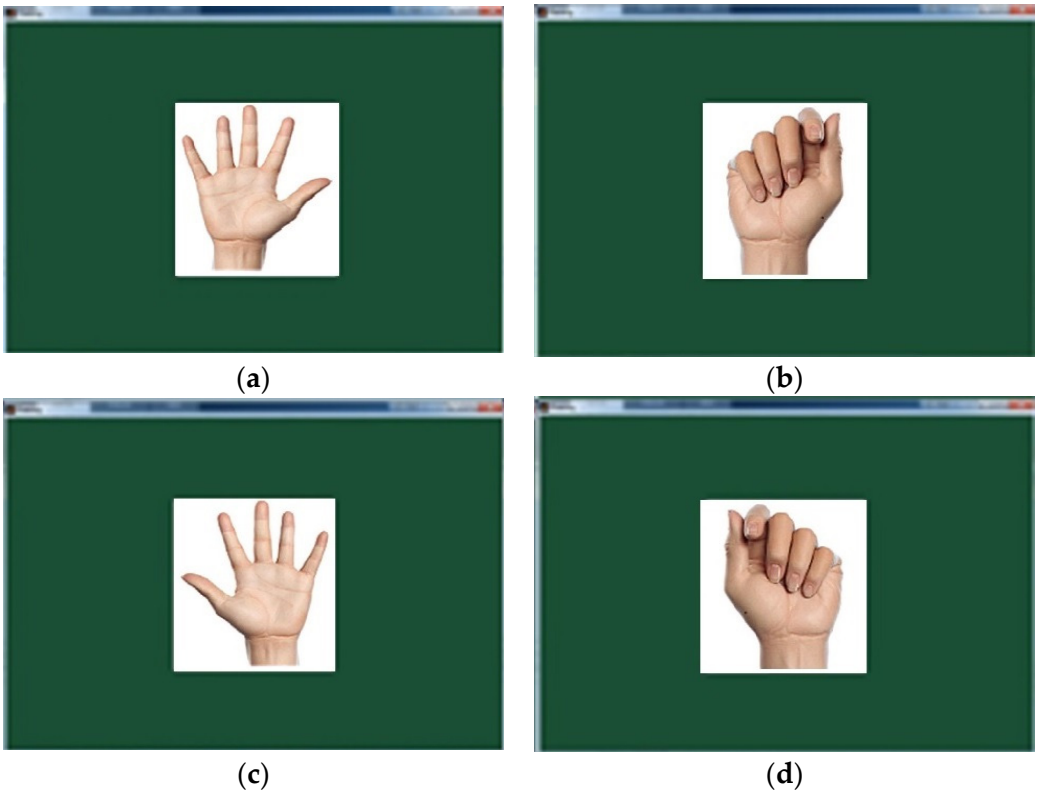


Figure 5. Display on screen showing (**a**) right-hand opening; (**b**) right-hand closing; (**c**) left-hand opening; and (**d**) left-hand closing.

2.7. Validation on the Public Datasets

To confirm the results from our dataset, two public datasets were used for validation. The first dataset was BCI competition IV dataset 2A [71]. This dataset collected EEG data from 9 subjects. EEG signals were recorded from 22 electrodes (Fz, FC3, FC1, FCz, FC2, FC4, C5, C3, C1, Cz, C2, C4, C6, CP3, CP1, CPz, CP2, CP4, P1, Pz, P2, and POz), arranged according to the international 10/20 system. This dataset does not contain EEG signals from F3, F4, P3, P4, T7, and T8 positions, which were collected in our dataset. Therefore, the nearest available electrode positions, namely FC3, FC4, CP3, CP4, C5, and C6, were selected in place of F3, F4, P3, P4, T7, and T8, respectively.

The second dataset was BCI competition III dataset Iva [72]. This dataset collected EEG data from 5 subjects. EEG signals were recorded from 118 electrodes at positions of the extended international 10/20 system. Comparing classification accuracies according to all designated groups of electrodes was validated on both datasets.

The electrodes of the first dataset were grouped as in our dataset: the two-, the three-, and the 5B-electrode groups. Other groups of electrodes were grouped differently as in our dataset as shown in Figure 6. The blue dots indicate the chosen electrodes for each group:

A group of five electrodes, comprising C5, C3, Cz, C4, and C6—this group was referred to as 5A_1.
A group of nine electrodes, comprising FC3, FCz, FC4, C3, Cz, C4, CP3, CPz, and CP4—this group was referred to as 9A.
A group of eleven electrodes, comprising FC3, FCz, FC4, C5, C3, Cz, C4, C6, CP3, CPz, and CP4—this group was referred to as 11A.
A group of thirteen electrodes, comprising Fz, FC3, FCz, FC4, C5, C3, Cz, C4, C6, CP3, CPz, CP4, and Pz—this group was referred to as 13.
A group of fifteen electrodes, comprising FC3, FC1, FCz, FC2, FC4, C3, C1, Cz, C2, C4, CP3, CP1, CPz, CP2, and CP4—this group was referred to as 15.

A group of twenty-one electrodes, comprising Fz, FC3, FC1, FCz, FC2, FC4, C5, C3, C1, Cz, C2, C4, C6, CP3, CP1, CPz, CP2, CP4, P1, Pz, and P2—this group was referred to as 21 (POz was not chosen because we focused on the positions along the center of the scalp between Fz and Pz in the vertical line).

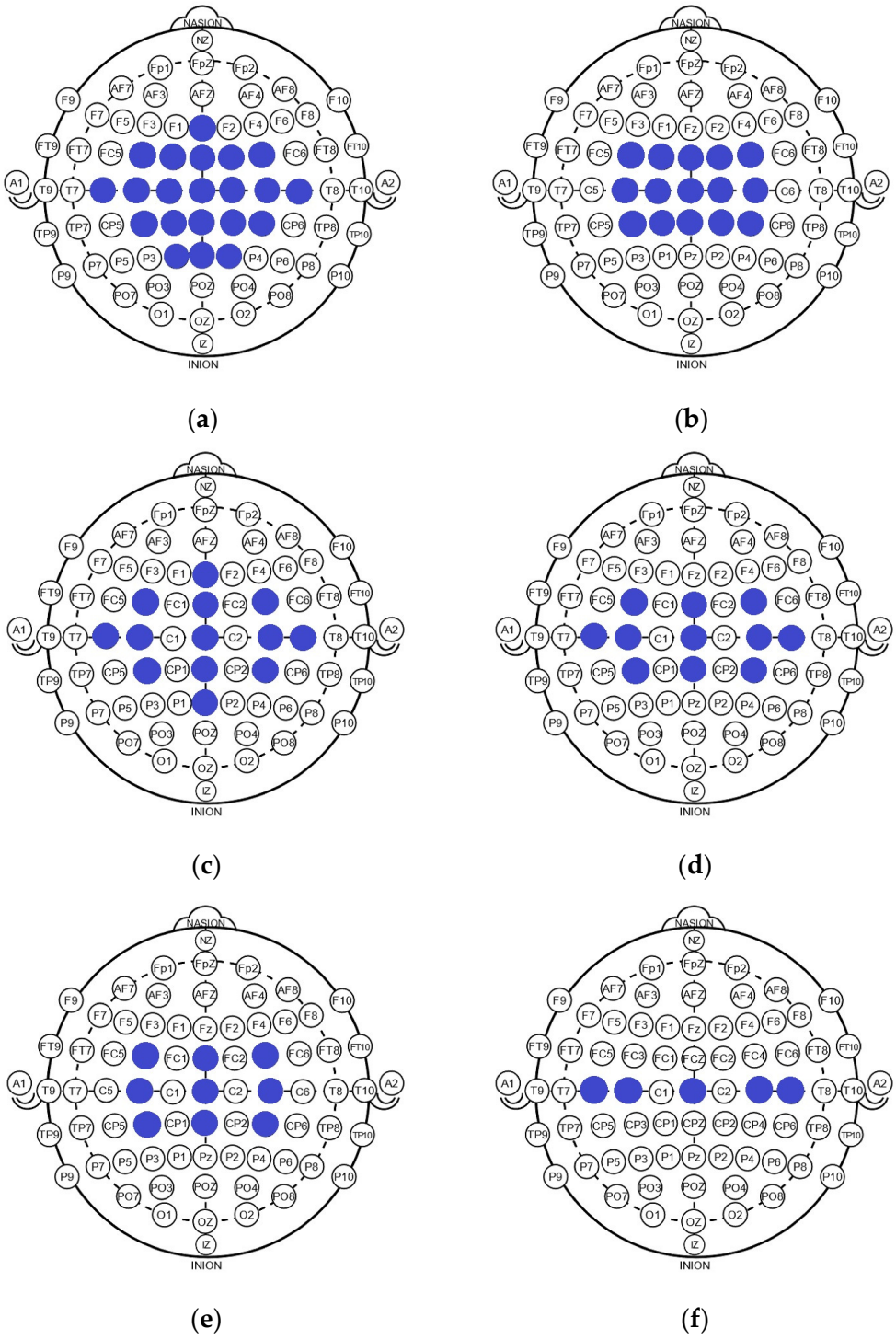


Figure 6. Additional groups of electrodes for dataset 1: (**a**) Group of twenty-one; (**b**) Group of fifteen; (**c**) Group of thirteen; (**d**) Group of 11A; (**e**) Group of 9A; (**f**) Group of 5A_1.

The electrodes of the second dataset were grouped as in our dataset and as in the first dataset, which were the three-, the 5A-, the 5B-, the nine-, the eleven-, the thirteen-, and the fifteen-electrode groups. Other groups of electrodes were grouped differently as in our

dataset and as in the first dataset as shown in Figure 7. The blue dots indicate the chosen electrodes for each group:

A group of twenty-five electrodes, comprising F3, F1, Fz, F2, F4, FC3, FC1, FCz, FC2, FC4, C3, C1, Cz, C2, C4, CP3, CP1, CPz, CP2, CP4, P3, P1, Pz, P2, and P4—this group was referred to as 25.

A group of forty-one electrodes, comprising F3, F1, Fz, F2, F4, FFC3, FFC1, FFC2, FFC4, FC3, FC1, FCz, FC2, FC4, CFC3, CFC1, CFC2, CFC4, C3, C1, Cz, C2, C4, CCP3, CCP1, CCP2, CCP4, CP3, CP1, CPz, CP2, CP4, PCP3, PCP1, PCP2, PCP4, P3, P1, Pz, P2, and P4—this group was referred to as 41.

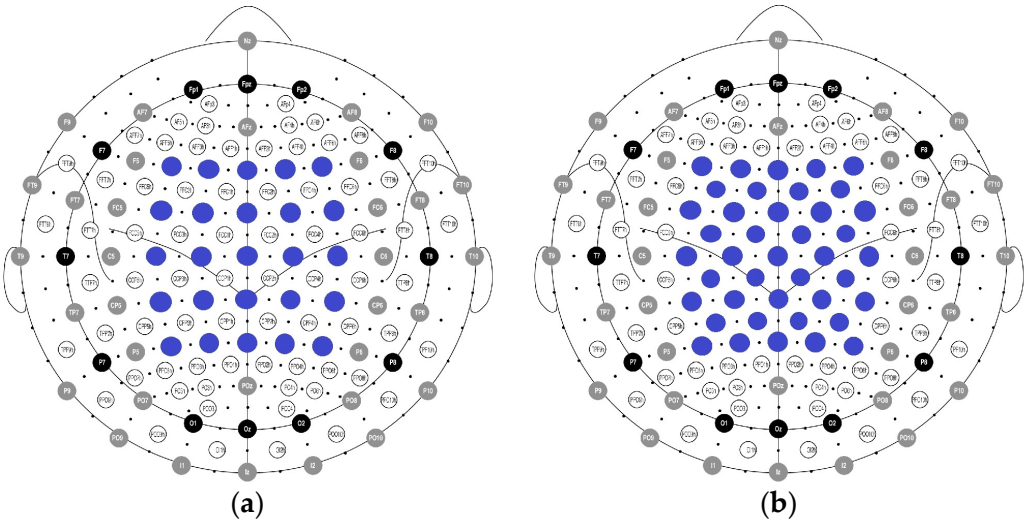


Figure 7. Additional groups of electrodes for dataset 2: (**a**) Group of twenty-five; (**b**) Group of forty-one.

The interpolation experiment was validated on only the second dataset, since the first dataset does not contain EEG signals from F3, F4, P3, and P4 positions, which are different from our dataset. In this validation, the electrodes were grouped as mentioned earlier, which were the three-, the 5A-, the 5B-, the nine-, the eleven-, the thirteen-, the fifteen-, the twenty-five, and the forty-one-electrode groups. Only the EEG signal at the Cz position was interpolated using the signals from electrodes surrounding it. For example, Cz was interpolated from C3 and C4 in the three-electrode group.

3. Results

The results from our dataset are presented as classification accuracies for classifying left- and right-hand movement during the opening/closing task. The classification parameters were the session-dependent experiment with varying electrode numbers using the FB feature. The statistical analysis involved a paired *t*-test and ANOVA with Bonferroni correction performed using IBM SPSS Statistics (Version 25). The significance level was set at 5% or a *p*-value of 0.05 for all statistical analyses.

Table 1 shows the average classification accuracy of all sessions for each participant. The classification accuracy was between approximately 60% and 80% for eight participants (S2, S4, S5, S6, S7, S8, S10, and S11). Accuracies of more than 80% were observed in three participants (S1, S3, and S9). The groups with nine and eleven electrodes yielded more than 75% accuracy for most participants.

Table 1. Classification accuracies of each participant.

Participant	Group of Electrodes					
	11	**9**	**5B**	**5A**	**3**	**2**
S1	85.78	82.34	73.09	77.73	66.05	58.91
S2	79.61	76.76	73.20	75.98	68.59	59.02
S3	81.41	78.24	76.37	74.65	71.88	66.48
S4	79.96	76.88	70.35	71.60	63.98	58.87
S5	75.63	76.72	72.15	68.52	68.95	61.37
S6	72.27	70.00	68.79	72.54	66.60	66.33
S7	76.99	74.06	73.24	73.05	67.30	64.30
S8	76.48	75.63	71.52	72.89	68.16	58.36
S9	82.38	78.01	74.34	77.97	66.88	63.09
S10	75.98	77.90	75.49	75.58	72.54	65.18
S11	77.58	74.02	69.22	71.68	62.70	57.81

Figure 8 shows the results of the statistical analysis comparing classification accuracies according to variation in electrode number. The average classification accuracies for each group of electrodes for all participants are shown. The eleven-electrode group showed the highest classification accuracy, while the two-electrode group showed the lowest. A greater number of electrodes tended to correlate with higher classification accuracy. Groups 5A and 5B showed comparable classification accuracy for all participants. Similar results could also be observed for groups of eleven and nine electrodes. The classification accuracy from the two-electrode group was significantly lower than that of the remaining groups. The classification accuracies of groups 5A and 5B were significantly higher than the classification accuracy of the three-electrode group, but there was no significant difference between groups 5A and 5B. The classification accuracies of groups with eleven and nine electrodes were significantly higher than the classification accuracy of the 5B group. There was no significant difference in the classification accuracy between groups with eleven and nine electrodes.

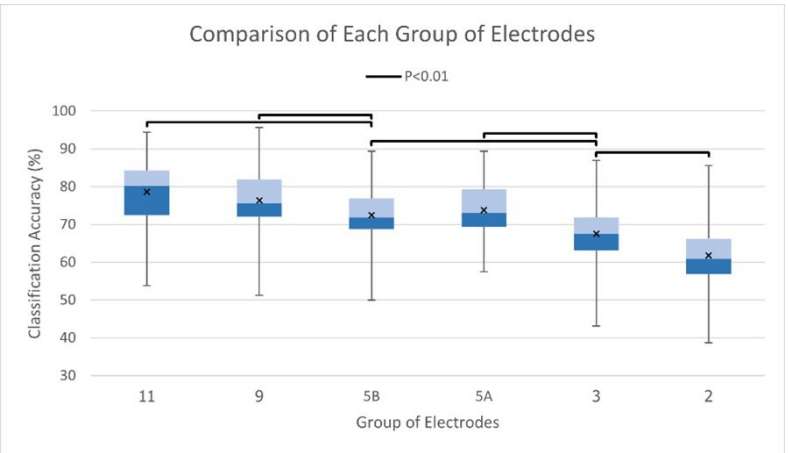


Figure 8. Statistical comparison for each electrode group from our dataset. 'x' denotes average classification accuracy, colored seams denote the median and the black line '-' above the plots represents statistically differences between groups, with a *p*-value less than 0.01.

Figure 9 shows the results of the statistical analysis comparing classification accuracies according to variation in electrode number from dataset 1. The validation results were analyzed using ANOVA with Bonferroni correction. The results show that a greater number of electrodes gives a higher classification accuracy. The twenty-one-electrode group showed the highest classification accuracy, while the two-electrode group showed the lowest. A greater number of electrodes tended to correlate with a higher classification accuracy. A significant difference was observed between the classification accuracy of the groups of

two/three electrodes and nine/eleven electrodes. This significant level from the public dataset agrees with the results from our dataset, which stated that the groups of nine and eleven electrodes gave significantly better accuracy than the fewer electrode groups. Furthermore, there were also no significant differences between the group of nine and eleven electrodes. This finding also corresponds to the results from our dataset. It should be noted that the difference between the group of five and nine electrodes was not significant in the public dataset 1, as opposed to our dataset results.

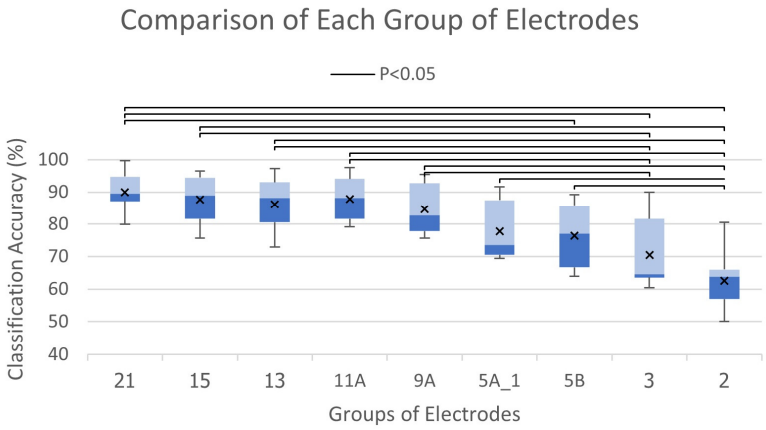


Figure 9. Statistical comparison for each electrode group from dataset 1. 'x' denotes average classification accuracy, colored seams denote the median and the black line '-' above the plots represents statistically significant differences between groups, with a *p*-value less than 0.05.

Figure 10 shows the results of the statistical analysis comparing classification accuracies according to variation in electrode number from dataset 2. The validation results were analyzed using ANOVA with Bonferroni correction. The results also show that a greater number of electrodes gives a higher classification accuracy. The three-electrode group showed the lowest classification accuracy. More electrodes also tended to correlate with a higher classification accuracy. The exception was the thirteen-electrode group, which provided the highest classification accuracy. The classification accuracy of the group of 5A was comparable to that of the group of 5B. The accuracies of classification among the remaining groups of electrodes, which were the groups of nine, eleven, thirteen, fifteen, twenty-five, and forty-one electrodes, were not significantly different. These results were consistent with the results from our dataset. However, the difference between electrode groups here was not significant, which was not consistent with the results from our dataset.

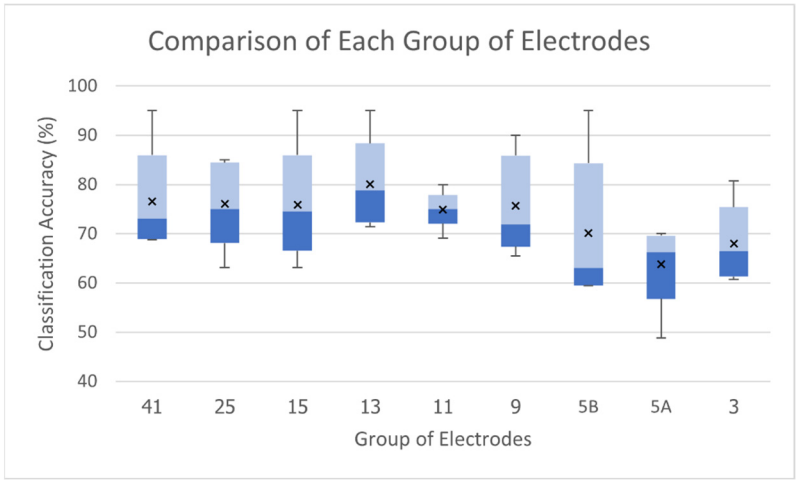


Figure 10. Statistical comparison for each electrode group from dataset 2. 'x' denotes average classification accuracy and colored seams denote the median.

To investigate the possibility of applying interpolation and further reducing the number of EEG channels needed, we applied an SSI interpolation algorithm via two separate tests. In the first test, interpolation generated electrode data outside the scalp area of a group of collected electrodes. Hence, a wider group of electrode data could be obtained. Interpolation was performed on the group of 5B electrodes. Although groups 5A and 5B showed comparable classification accuracies according to Figure 8, we chose the 5B group as it covers the central area of the scalp, while the T7 and T8 electrodes in the 5A group were closer to the ears. Interpolated data were generated from the 5B group. The interpolation outputs were the interpolated group of eleven electrodes and the interpolated group of nine electrodes.

In the interpolated group of eleven electrodes, F3, F4, T7, T8, P3, and P4 positions were interpolated from Fz, C3, Cz, C4, and Pz positions. Positions F3, F4, P3, and P4 were part of the interpolated group of nine electrodes. Hence, the interpolated groups of eleven and nine electrodes covered the same positions as the corresponding measured groups, shown in Figure 2.

Figure 11 shows the comparison of classification accuracies for the measured group of eleven electrodes and interpolated group of eleven electrodes. Figure 12 shows the comparison of classification accuracies for the measured group of nine electrodes and interpolated group of nine electrodes. The classification accuracies of the measured groups were clearly higher than those of the interpolated groups for all participants.

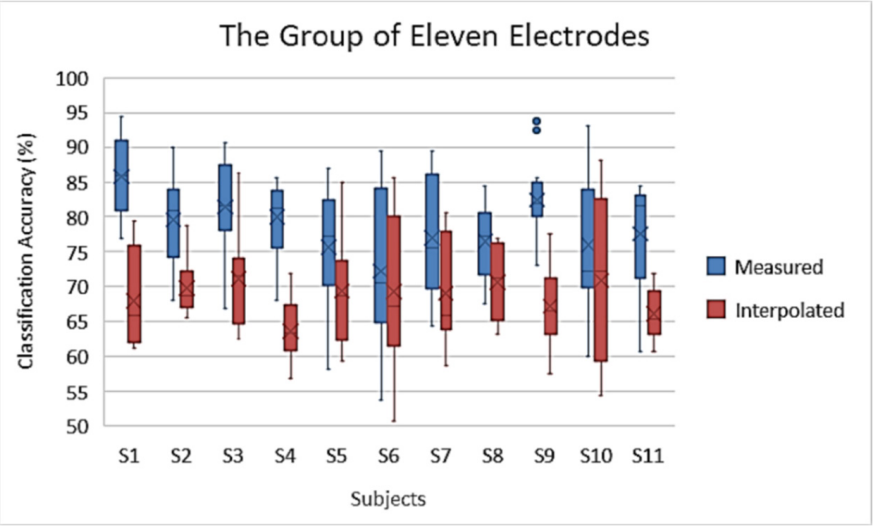


Figure 11. Comparison of measured and interpolated eleven-electrode group. 'x' denotes average classification accuracy, '-' denotes median, and dots represent outliers.

The comparison of the classification accuracies of the measured and interpolated groups of electrodes was performed using a paired *t*-test. The significance level was set to a *p*-value of 0.05, and the statistical outputs are shown in Table 2. We found significant differences in the classification accuracies for both groups. Moreover, the classification accuracies for both interpolated groups were comparable, most likely due to EEG data interpolated from the same group of electrodes, which were FZ, C3, Cz, C4, and Pz.

In the second test, interpolation generated electrode data within a group of collected electrodes. Therefore, grouped electrode data closer together were retained. We chose a group of nine collected electrodes: F3, Fz, F4, C3, Cz, C4, P3, Pz, and P4. Three combined groups of collected and interpolated electrodes comprised 13, 15, and 25 electrodes.

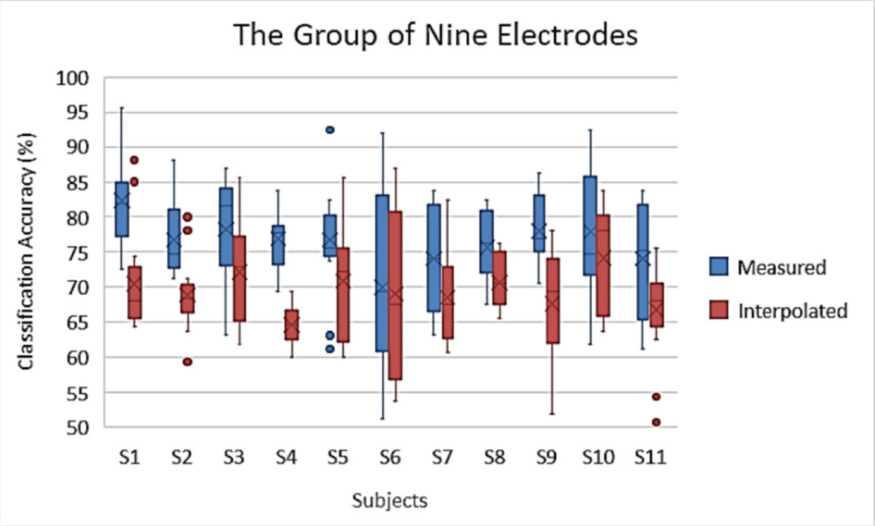


Figure 12. Comparison of measured and interpolated nine-electrode group. 'x' denotes average classification accuracy, '-' denotes median, and dots represent outliers.

Table 2. Statistical results of measured and interpolated groups of electrodes.

Combined Group of Electrodes	Classification Accuracy ± S.D.		*p*-Value
	Measured	Interpolated	
11	78.58 ± 8.15	68.62 ± 7.29	$p < 0.01$
9	76.40 ± 7.94	69.38 ± 7.34	$p < 0.01$

According to Figure 13, the group of thirteen electrodes consisted of the four positions of interpolated electrodes, which were FC1, FC2, CP1, and CP2. For the group of fifteen electrodes, we interpolated F1, F2, C1, C2, P1, and P2 positions. For the group of twenty-five electrodes, we interpolated F1, F2, FC3, FC1, FCz, FC2, FC4, C1, C2, CP3, CP1, CPz, CP2, CP4, P1, and P2 positions.

Figure 14 compares the classification accuracies of the measured and combined groups of electrodes in the increasing number of electrodes experiment. Measured electrodes were represented by blue dots, interpolated electrodes were represented by red dots, and combined electrodes (including both measured and interpolated) were represented by green dots. The classification accuracies of the measured group of nine electrodes were clearly higher than those of the three combined groups of thirteen, fifteen, and twenty-five electrodes for all participants. The results of the three combined groups were comparable for all participants, although the classification accuracies for the group of thirteen electrodes were slightly higher than those of all other groups.

Table 3 shows the average classification accuracies with standard deviations for all participants. The classification accuracies were compared with the measured group of nine electrodes. The statistical results were calculated using a paired *t*-test. The classification accuracy of the measured group of nine electrodes was significantly higher than that of the combined electrode groups. However, the classification accuracies of all combined groups of electrodes were not significantly different, which was consistent with the results of the first experiment using interpolation. A lower number of interpolated channels of electrodes showed comparable classification accuracies for a higher number of interpolated electrode channels.

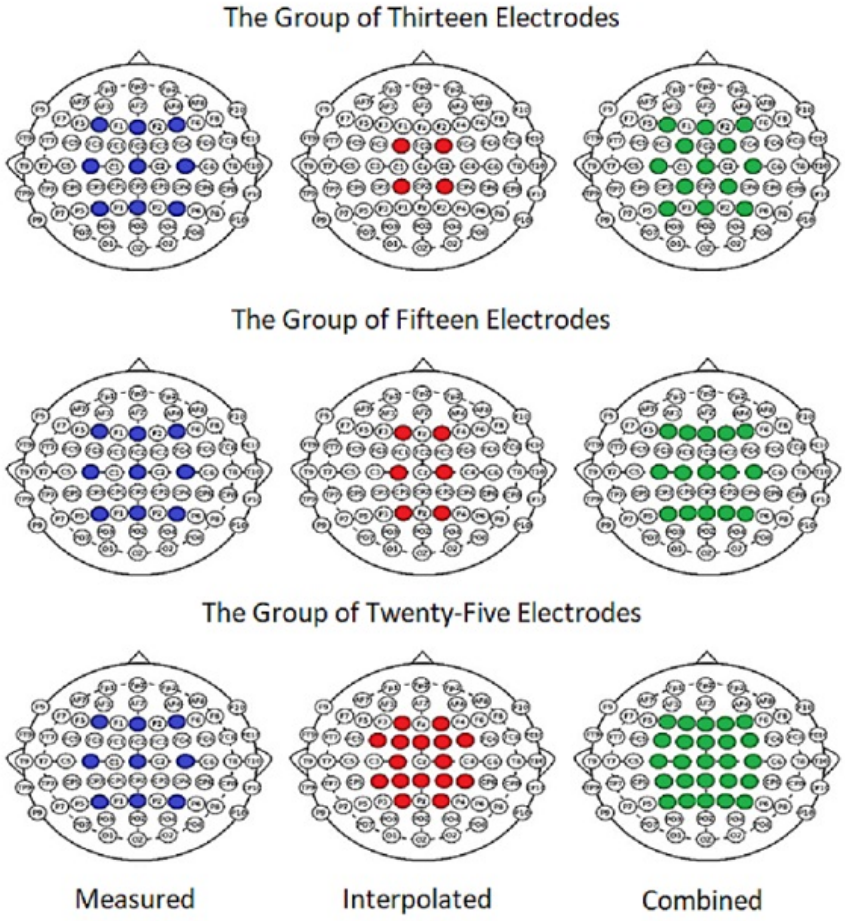


Figure 13. Groups of combined electrodes.

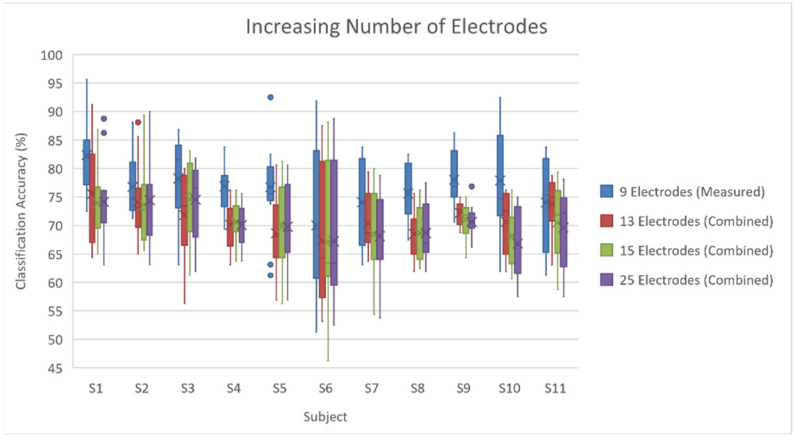


Figure 14. Comparison of classification accuracy with increasing number of electrodes. 'x' denotes average classification accuracy, '-' denotes median, and dots represent outliers.

Table 3. Statistical results of classification accuracies of combined groups of electrodes.

Combined Group of Electrodes	Classification Accuracy ± S.D.	*p*-Value
13	71.19 ± 6.94	$p < 0.01$
15	70.60 ± 7.23	$p < 0.01$
25	70.41 ± 7.29	$p < 0.01$

The validation of interpolation results was conducted in two tests. The first test was to directly compare the signal between measured Cz and interpolated Cz; the difference of the signals was calculated sample-by-sample. The root mean square (RMS) was then used as the comparison results as shown in Figure 15. The statistical analysis results were performed by using ANOVA with Bonferroni correction. The second test was to compare the classification accuracies of the measured groups and combined groups of electrodes as shown in Table 4. The comparison results were analyzed using a paired *t*-test.

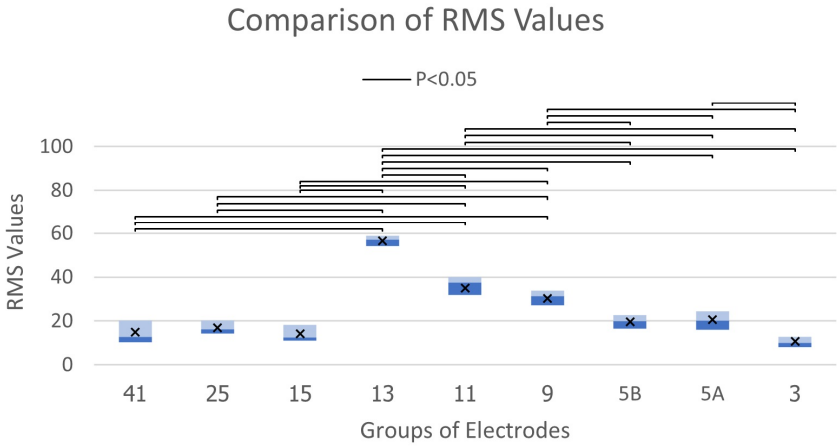


Figure 15. Comparison of RMS values of each group of electrodes. 'x' denotes average classification accuracy, colored seams denote the median and the black line '-' above the plots represents significant differences between groups, with a *p*-value less than 0.05.

Table 4. Statistical results classification accuracies of measured groups and combined groups of electrodes.

Group of Electrodes	Classification Accuracy ± S.D.		*p*-Value
	Measured	Interpolated	
Average	73.45 ± 10.30	68.23 ± 12.6	$p < 0.01$

The results from Figure 15 show that a small (3–5) and large (15–41) number of electrodes provided an interpolated Cz close to the measured Cz. The number of electrodes in between (9–13) yielded significantly inaccurate results. The results show that a larger number of electrodes did not make the interpolated signal closer to the actual measured signal. On the contrary, the RMS values were increased as observed in the three-, the 5A-, the 5B-, the nine-, the eleven-, and the thirteen-electrode groups. However, the RMS values seem comparable between the three-, the fifteen-, the twenty-five-, and the forty-one-electrode groups. From Table 4, the average classification accuracies from measurement were significantly higher than those from the combined groups of electrodes, which was consistent with the results from our dataset.

4. Discussion

We present the results from our dataset according to variations in the number of electrodes using the FB feature depending on session. The classification accuracies of all sessions for all participants were averaged and grouped by electrode group.

Significant differences in the classification accuracies between the two- and three-electrode groups suggest that the Cz position is important for classifying the left- and right-hand opening/closing task. Groups 5A and 5B explored the effect of the EEG signal between two added positions of electrodes in both groups, namely positions T7 and T8 in the 5A group and Fz and Pz in the 5B group. Although the classification accuracies of the 5A group were higher than those of the 5B group, the difference was not statistically

significant. The classification accuracies of both groups showed significantly higher classification accuracies than those of the three-electrode group. This could be interpreted as T7, T8, Fz, and Pz positions strongly affecting classification of the left- and right-hand opening/closing task.

The classification accuracies for the nine- and eleven-electrode groups were significantly higher than those of the 5A and 5B groups, as observed in Figure 8, which confirmed our hypothesis as accuracy tends to improve with increasing channel number [73]. There were no significant differences in the classification accuracies between the groups of eleven and nine electrodes. Therefore, we can conclude that adding F3, F4, P3, and P4 to the five-electrode group to form nine electrodes significantly increases the classification accuracy of left- and right-hand opening/closing tasks. This experiment showed that all electrode positions designated for each group of electrodes contained meaningful information to efficiently classify left- and right-hand opening/closing tasks beside positions C3 and C4.

The difference in the classification accuracies of these groups of electrodes may be attributed to the spatio-temporal dynamics of the EEG during the hand opening/closing motor imagery task. The spatial distribution measured with EEG was reported to vary during movement-related activity, depending on the frequency band [74–76]. Our results indicated that the changes in EEG occurred from the frontal (F3, Fz, F4) to parietal (P3, Pz, P4) regions, which is consistent with many studies [62,77,78]. In addition, the results from these studies [36,51] show that filtering brain rhythms into a frequency filter (FB) provides good classification accuracy. This suggested that meaningful information about EEG activity is frequency-related. Therefore, in MI-based BCI, especially with a limited number of EEG channels, it is necessary to consider the channel configuration that corresponds to each MI task.

We also measured the setup times for each participant and found that more than 30 min always made the participants uncomfortable and moody. The setup process involved attaching electrodes, confirming proper contact with the scalp, and visually verifying EEG signal quality. If the signal was flat or noisy, the attachment and contact-checking steps were repeated. The eleven-electrode group took a minimum of 15 min to setup, the nine-electrode group took 10–15 min, and the five-electrode group took less than 10 min. For classification accuracies, the eleven- or nine-electrode groups were selected when using an EEG device with a low number of channels. However, the nine-electrode group was preferred due to the quicker setup time.

The results from the two public datasets generally correlate with the conclusions from our dataset. All the dataset results confirmed the perception that the larger number of electrodes gives higher classification accuracy. The groups of nine and eleven electrodes yield significantly higher accuracy than the groups of two and three electrodes in the public dataset 1 and our dataset. The difference between the group of nine and eleven electrodes was not significant in all three datasets. Hence, our recommended minimal number of electrodes remains nine.

For the interpolation experiments, the interpolation results did not yield improved classification accuracy from the measured data. An explanation may be that interpolation is designed to repair signals from poor EEG channels. One interpolated channel is normally computed from a large number of surrounding channels [69,79,80]. Here, six or more channels were interpolated using EEG signals of scalp potential from five electrodes. It is possible that too many electrodes were interpolated from too few collected data points in this test. As a result, the quality of the interpolated data may suffer, which could result in the loss of important classification features and may contribute to the low classification accuracies observed in the combined groups.

According to Figure 14, interpolation provided comparable classification accuracies between the measured and combined groups of electrodes in one participant (S6), while the interpolated groups of electrodes showed poorer classification accuracies for most participants. According to other studies [34,36,38,81], ERD/ERS phenomena are participant-specific, whereby phenomena can occur in different positions and different frequencies

for each participant. This may be explained by the corresponding brain area that contains meaningful information for classifying the left- and right-hand opening/closing task in participant S6 that was not part of the interpolated channels.

The validation results were also consistent with the results from our dataset, showing that there were significant differences in the classification accuracy between the measured- and combined groups of electrodes, although the interpolation validation was different from the interpolation experiment in the interpolation experiment in which many EEG signals were interpolated. The combined groups of electrodes, which consisted of one interpolated EEG signal, did not give comparable classification accuracy to that of the measured groups of electrodes. Therefore, the validation of many interpolated EEG signals, as in the interpolation experiment, was not necessary. The results were also consistent with the results from our dataset, showing that there were significant differences in classification accuracy between the measured and combined groups of electrodes. The RMS results might indicate that a sufficient number of EEG signals was required to ensure that the difference between the interpolated signal and the actual measured signal was relatively constant, which was fifteen positions or more. Moreover, the RMS values that were not significantly different between the groups of 5A and 5B and between the nine- and eleven-electrode groups were probably the reason why the classification accuracy of groups 5A and 5B and that of the nine- and eleven-electrode groups were comparable. The conclusion was that generating additional EEG data through the SSI interpolation technique did not improve classification accuracy.

EEG is a BCI technology that has been proven to be harmless to users [82]. Furthermore, MI requires no actual body movement, so MI training using BCI can be considered safe. The application of BCI in MI training and exercise is still either in the research stage or under the supervision of medical experts. To implement the system in real-world settings, some practical measures should be considered. These include maintaining a comfortable distance between the participant and the screen (50–100 cm), and the chair should well support a participant's body and have a backrest and armrests. Common feedback from healthy participants from this work and patients from the experiment in [83], which one of the authors assisted in data collection, was that the session duration should be short. The MI experiments from the literature were kept below one and a half hours [12,14,15,18,55]. Furthermore, from our experience, the setup time should not exceed 30 min to avoid the subject being uncomfortable and unwilling to cooperate in the experiments. Therefore, relaxation and fatigue levels, indicating the participants' comfort, are important variables in the context of wearable devices because these variables affect the performance of the system. In addition, the characteristics of the headset and electrode, such as the material, weight, as well as clean and care, also affect the setup time and wearability. In this study, we used a g.Nautilus headset, which has a fabric headset (cap) combined with dry electrodes. The users' verbal feedback was that it was acceptable because it took 10–15 min to set up and needed no hair cleaning after use. Conductive gel-based electrodes tend to leave residue on the hair, which requires hair washing after use.

5. Limitations and Further Work

The small sample size and diversity of participants, including gender and individuals with neurological conditions, can be considered limitations of this study. Although a larger sample size should give more reliable results, our results were comparable to those from some studies with a small number of participants [84–86].

While the study by Alimardani et al. stated that there is no research that has clearly shown that gender affects the ability to perform motor imagery, participants' relaxation level and fatigue show a significant difference in BCI performance between users [87].

Recruiting participants with or without neurological conditions depends on the application of interest. For MI-based BCI applications, the phenomena that occur when performing motor imagery are ERD and ERS, which can occur in both healthy participants and patients with neurological disease [87]. Moreover, many studies have shown that MI-

based BCI applications are also beneficial for the normal elderly [88–90]. Thus, recruiting healthy participants is a good starting point for system development.

Variability in individual EEG patterns is also one of the concerns in developing BCI applications due to the non-stationary characteristic of EEG, as mentioned in the Introduction section. It is a noisy and high-variance signal. Relieving the effect of the non-stationary characteristic of EEG, CSP, and SVM are the feature extraction algorithm and the classifier that are suitable to handle the EEG signal, as discussed in the Introduction section. The session-dependent paradigm could also help with the non-stationary characteristic of EEG.

This study aims to investigate the feasibility of using the minimum number of channels on an EEG device to develop a BCI application that provides acceptable performance in a relatively short setup time. Further work could be needed to realize a system with better performance given the same setup time by considering different classification parameters, such as channel selection techniques, features, and classifiers. For example, instead of the SSI algorithm, a method known as the inverse problem can also be used to investigate the minimum number of electrodes required. The inverse problem estimates a number of sources much larger than the number of available sensors. Generated EEG data are then computed using estimated sources [91,92], thus improving spatial resolution. Minimum-norm solutions, beamformers, and dipole modeling are other popular methods that show good results in classifying MI tasks [92].

Another alternative method to improve MI classification accuracy in minimal channel setup is adding imperceptible vibratory stimulus. Studies showed that subthreshold stimulation increased ERD activity during actual body movement [93] and KMI [94]. ERD enhancement could help improve classification accuracy, so the method warrants further investigation. This approach requires a tiny stimulus device that is attached to an index finger.

Furthermore, deep neural networks (DNNs) have also gained considerable research attention, including EEG-based BCI systems [32]. Convolutional neural networks (CNNs) are the most popular BCI method, and many studies show CNNs can outperform linear classifiers, such as LDA or SVM, which are well-established for EEG-based BCI [32,91,95]. However, most of these studies were offline, so CNN performance for online applications needs to be further investigated. DNNs, on the other hand, may not perform well for BCI applications, mostly due to a limited amount of training data [32]. Although theoretically there is no minimum dataset size, larger datasets return higher classification accuracy and a more reliable system [96,97]. Therefore, when choosing a DNN as a classifier, long-term data collection, involving a larger number of participants, requires adequate planning.

Moreover, the study by Aliakbaryhosseinabadi et al. suggested that, for detecting movement intention, the classification should be performed in a subject-specific manner by selecting the optimal combination of task-related features, classifier, and EEG channel for each subject [98]. These results could be used as guidelines, combined with the findings from our study, to further explore the possibilities of optimizing the EEG channel number and locations based on subject-specific task-related activity.

6. Conclusions

A key factor, when considering wearable devices, is wearability. The number of channels in an EEG device adversely impacts the setup time, whereby a greater number of channels results in a longer setup time. Using the FB feature and session-dependent training, investigating the number of available channels can help develop a successful BCI application using minimal channels. Other interpolation techniques and inverse problem solutions that can approximate additional electrode data from nearby electrodes should also be explored.

Our results show that all designated positions of the electrodes in each group of electrodes contained meaningful information to efficiently classify left- and right-hand opening/closing tasks in addition to the C3 and C4 positions. Significant differences

in classification accuracies between the groups of two and three electrodes suggest the importance of obtaining EEG data from the Cz position, while the results from groups 5A and 5B highlighted the significance of EEG data from positions T7, T8, Fz, and Pz. The results of the nine- and the five-electrode groups also indicated the importance of obtaining EEG data from positions F3, F4, P3, and P4.

All groups of five or more electrodes returned acceptable accuracies when classifying left- and right-hand opening/closing MI tasks (more than 70%) [18]. Furthermore, the results from the two public datasets generally correlated with the conclusions from our dataset. All the dataset results confirmed the perception that the larger number of electrodes gives higher classification accuracy. The nine-electrode group gave comparable results to the eleven-electrode groups. Hence, our recommended minimal number of electrodes is nine due its shorter setup time compared with the eleven-electrode groups, despite their non-significant differences in classification accuracy. Finally, the interpolation results from our dataset and from the second public dataset were also consistent. The results showed that the classification accuracy of the measured group of electrodes was significantly higher than that of the interpolated and combined group of electrodes. This might suggest that the spherical spline interpolation (SSI) algorithm may not be suitable for generating additional EEG data to enhance classification performance. Hence, a sufficient number of EEG signals need to be collected without relying on generated data.

Author Contributions: A.S. conceived, designed, and conducted the experiments and wrote the manuscript. S.P.-n. designed the experiments and wrote and revised the manuscript. P.I. conceived the project, contributed experiment equipment, and drafted the manuscript. All authors have read and agreed to the published version of the manuscript.

Funding: This research was supported by the 90th Anniversary of Chulalongkorn University, Ratchadapisek Sompote Fund, grant number GCUGR1125601029D.

Data Availability Statement: The datasets for this study can be found in the Dryad Digital Repository https://datadryad.org/stash/share/tfHXksEwRJS1Sakmrm8JN9kf1iLVXMnn_m7WnSIMJYs (accessed on 15 February 2022).

Conflicts of Interest: The authors declare that the research was conducted in the absence of any commercial or financial relationships that could be construed as potential conflicts of interest.

References

1. Glaros, C.I.; Fotiadis, D. *Wearable Devices in Healthcare*; Springer: Berlin, Heidelberg, 2005; pp. 237–264.
2. Case, M.A.; Burwick, H.A.; Volpp, K.G.; Patel, M.S. Accuracy of Smartphone Applications and Wearable Devices for Tracking Physical Activity Data. *JAMA* **2015**, *313*, 625–626. [CrossRef]
3. Patel, M.S.; Asch, D.A.; Volpp, K.G. Wearable devices as facilitators, not drivers, of health behavior change. *JAMA* **2015**, *313*, 459–460. [CrossRef]
4. Wang, R.; Blackburn, G.; Desai, M.; Phelan, D.; Gillinov, L.; Houghtaling, P.; Gillinov, M. Accuracy of Wrist-Worn Heart Rate Monitors. *JAMA Cardiol.* **2017**, *2*, 104–106. [CrossRef]
5. Looney, D.; Goverdovsky, V.; Rosenzweig, I.; Morrell, M.J.; Mandic, D.P. Wearable in-ear encephalography sensor for monitoring sleep. preliminary observations from Nap studies. *Ann. Am. Thorac. Soc.* **2016**, *13*, 2229–2233. [CrossRef] [PubMed]
6. Gu, Y.; Cleeren, E.; Dan, J.; Claes, K.; Van Paesschen, W.; Van Huffel, S.; Hunyadi, B. Comparison between Scalp EEG and Behind-the-Ear EEG for Development of a Wearable Seizure Detection System for Patients with Focal Epilepsy. *Sensors* **2018**, *18*, 29. [CrossRef] [PubMed]
7. Nakamura, T.; Goverdovsky, V.; Morrell, M.J.; Mandic, D.P. Automatic Sleep Monitoring Using Ear-EEG. *IEEE J. Transl. Eng. Health Med.* **2017**, *5*, 1–8. [CrossRef] [PubMed]
8. Zibrandtsen, I.; Kidmose, P.; Christensen, C.; Kjaer, T. Ear-EEG detects ictal and interictal abnormalities in focal and generalized epilepsy—A comparison with scalp EEG monitoring. *Clin. Neurophysiol.* **2017**, *128*, 2454–2461. [CrossRef] [PubMed]
9. Yuan, H.; He, B. Brain–computer interfaces using sensorimotor rhythms: Current state and future perspectives. *IEEE Trans. Biomed. Eng.* **2014**, *61*, 1425–1435. [CrossRef] [PubMed]
10. He, B.; Baxter, B.; Edelman, B.J.; Cline, C.C.; Ye, W.W. Noninvasive brain-computer interfaces based on sensorimotor rhythms. *Proc. IEEE* **2015**, *103*, 907–925. [CrossRef] [PubMed]
11. Soekadar, S.R.; Birbaumer, N.; Slutzky, M.W.; Cohen, L.G. Brain-machine interfaces in neurorehabilitation of stroke. *Neurobiol Dis.* **2015**, *83*, 172–179. [CrossRef] [PubMed]

12. Chaudhary, U.; Birbaumer, N.; Ramos-Murguialday, A. Brain–computer interfaces for communication and rehabilitation. *Nat. Rev. Neurol.* **2016**, *12*, 513–525. [CrossRef] [PubMed]
13. McFarland, D.J.; Wolpaw, J.R. EEG-based brain–computer interfaces. *Curr. Opin. Biomed. Eng.* **2017**, *4*, 194–200. [CrossRef] [PubMed]
14. Lazarou, I.; Nikolopoulos, S.; Petrantonakis, P.C.; Kompatsiaris, I.; Tsolaki, M. EEG-based brain–computer interfaces for communication and rehabilitation of people with motor impairment: A novel approach of the 21st century. *Front. Hum. Neurosci.* **2018**, *12*, 14. [CrossRef]
15. Ang, K.K.; Guan, C. Brain-Computer Interface in Stroke Rehabilitation. *J. Comput. Sci. Eng.* **2013**, *7*, 139–146. [CrossRef]
16. Mrachacz-Kersting, N.; Jiang, N.; Stevenson, A.J.T.; Niazi, I.K.; Kostic, V.; Pavlovic, A.; Radovanovic, S.; Djuric-Jovicic, M.; Agosta, F.; Dremstrup, K.; et al. Efficient neuroplasticity induction in chronic stroke patients by an associative brain-computer interface. *J. Neurophysiol.* **2016**, *115*, 1410–1421. [CrossRef] [PubMed]
17. Frolov, A.A.; Mokienko, O.; Lyukmanov, R.; Biryukova, E.; Kotov, S.; Turbina, L.; Nadareyshvily, G.; Bushkova, Y. Post-stroke Rehabilitation Training with a Motor-Imagery-Based Brain-Computer Interface (BCI)-Controlled Hand Exoskeleton: A Randomized Controlled Multicenter Trial. *Front. Neurosci.* **2017**, *11*, 400. [CrossRef]
18. Ang, K.K.; Guan, C.; Chua, K.S.G.; Ang, B.T.; Kuah, C.W.K.; Wang, C.; Phua, K.S.; Chin, Z.Y.; Zhang, H. A Large Clinical Study on the Ability of Stroke Patients to Use an EEG-Based Motor Imagery Brain-Computer Interface. *Clin. EEG Neurosci.* **2011**, *42*, 253–258. [CrossRef]
19. Pfurtscheller, G.; Lopes da Silva, F.H. Event-related EEG/MEG synchronization and desynchronization: Basic principles. *Clin. Neurophysiol.* **1999**, *110*, 1842–1857. [CrossRef]
20. Nakayashiki, K.; Saeki, M.; Takata, Y.; Hayashi, Y.; Kondo, T. Modulation of event-related desynchronization during kinematic and kinetic hand movements. *J. Neuroeng. Rehabilitation* **2014**, *11*, 90. [CrossRef]
21. Klimesch, W. EEG alpha and theta oscillations reflect cognitive and memory performance: A review and analysis. *Brain Res. Rev.* **1999**, *29*, 169–195. [CrossRef]
22. Friese, U.; Daume, J.; Göschl, F.; König, P.; Wang, P.; Engel, A.K. Oscillatory brain activity during multisensory attention reflects activation, disinhibition, and cognitive control. *Sci. Rep.* **2016**, *6*, 32775. [CrossRef]
23. Klimesch, W.; Schimke, H.; Schwaiger, J. Episodic and semantic memory: An analysis in the EEG theta and alpha band. *Electroencephalogr. Clin. Neurophysiol.* **1994**, *91*, 428–441. [CrossRef]
24. Malouin, F.; Richards, C.L.; Jackson, P.L.; Lafleur, M.F.; Durand, A.; Doyon, J. The kinesthetic and visual imagery questionnaire (KVIQ) for assessing motor imagery in persons with physical disabilities: A reliability and construct validity study. *J. Neurol. Phys. Ther.* **2007**, *31*, 20–29. [CrossRef]
25. Guillot, A.; Collet, C.; Nguyen, V.A.; Malouin, F.; Richards, C.; Doyon, J. Brain activity during visual versus kinesthetic imagery: An fMRI study. *Hum. Brain Mapp.* **2008**, *30*, 2157–2172. [CrossRef] [PubMed]
26. Ridderinkhof, K.R.; Brass, M. How kinesthetic motor imagery works: A predictive-processing theory of visualization in sports and motor expertise. *J. Physiol.* **2015**, *109*, 53–63. [CrossRef] [PubMed]
27. Decety, J.; Grèzes, J. Neural mechanisms subserving the perception of human actions. *Trends Cogn. Sci.* **1999**, *3*, 172–178. [CrossRef] [PubMed]
28. Behrendt, F.; Zumbrunnen, V.; Brem, L.; Suica, Z.; Gäumann, S.; Ziller, C.; Gerth, U.; Schuster-Amft, C. Effect of motor imagery training on motor learning in children and adolescents: A systematic review and meta-analysis. *Int. J. Environ. Res. Public Health* **2021**, *18*, 9467. [CrossRef] [PubMed]
29. Choi, J.W.; Kim, B.H.; Huh, S.; Jo, S. Observing actions through immersive virtual Reality enhances motor imagery training. *IEEE Trans. Neural Syst. Rehabil. Eng.* **2020**, *28*, 1614–1622. [CrossRef] [PubMed]
30. Juliano, J.M.; Spicer, R.P.; Vourvopoulos, A.; Lefebvre, S.; Jann, K.; Ard, T.; Santarnecchi, E.; Krum, D.M.; Liew, S.-L. Embodiment is related to better performance on a brain–computer interface in immersive virtual reality: A Pilot Study. *Sensors* **2020**, *20*, 1204. [CrossRef] [PubMed]
31. Lakshminarayanan, K.; Shah, R.; Daulat, S.R.; Moodley, V.; Yao, Y.; Madathil, D. The effect of combining action observation in virtual reality with kinesthetic motor imagery on cortical activity. *Front. Neurosci.* **2023**, *17*, 1201865. [CrossRef]
32. Lotte, F.; Bougrain, L.; Cichocki, A.; Clerc, M.; Congedo, M.; Rakotomamonjy, A.; Yger, F. A review of classification algorithms for EEG-based brain–computer interfaces: A 10 year update. *J. Neural Eng.* **2018**, *15*, 031005. [CrossRef]
33. Lotte, F.; Congedo, M.; Lécuyer, A.; Lamarche, F.; Arnaldi, B. A review of classification algorithms for EEG-based brain–computer interfaces. *J. Neural. Eng.* **2007**, *4*, R1. [CrossRef] [PubMed]
34. Müller-Gerking, J.; Pfurtscheller, G.; Flyvbjerg, H. Designing optimal spatial filters for single-trial EEG classification in a movement task. *Clin. Neurophysiol.* **1999**, *110*, 787–798. [CrossRef] [PubMed]
35. Blankertz, B.; Tomioka, R.; Lemm, S.; Kawanabe, M.; Muller, K.-R. Optimizing Spatial filters for Robust EEG single-trial analysis. *IEEE Signal Process. Mag.* **2007**, *25*, 41–56. [CrossRef]
36. Ang, K.K.; Chin, Z.Y.; Wang, C.; Guan, C.; Zhang, H. Filter Bank Common Spatial Pattern Algorithm on BCI Competition IV Datasets 2a and 2b. *Front. Neurosci.* **2012**, *6*, 39. [CrossRef] [PubMed]
37. Park, C.; Took, C.C.; Mandic, D.P. Augmented Complex Common Spatial Patterns for Classification of Noncircular EEG From Motor Imagery Tasks. *IEEE Trans. Neural Syst. Rehabil. Eng.* **2014**, *22*, 1–10. [CrossRef]

38. Meng, J.; Yao, L.; Sheng, X.; Zhang, D.; Zhu, X. Simultaneously optimizing spatial spectral features based on mutual information for EEG classification. *IEEE Trans. Biomed. Eng.* **2014**, *62*, 227–240. [CrossRef] [PubMed]
39. Jiang, J.; Wang, C.; Wu, J.; Qin, W.; Xu, M.; Yin, E. Temporal Combination Pattern Optimization Based on Feature Selection Method for Motor Imagery BCIs. *Front. Hum. Neurosci.* **2020**, *14*, 231. [CrossRef]
40. Pei, Y.; Luo, Z.; Zhao, H.; Xu, D.; Li, W.; Yan, Y.; Yan, H.; Xie, L.; Xu, M.; Yin, E. A Tensor-Based Frequency Features Combination Method for Brain–Computer Interfaces. *IEEE Trans. Neural Syst. Rehabil. Eng.* **2021**, *30*, 465–475. [CrossRef]
41. Muller, K.-R.; Anderson, C.; Birch, G. Linear and nonlinear methods for brain-computer interfaces. *IEEE Trans. Neural Syst. Rehabil. Eng.* **2003**, *11*, 165–169. [CrossRef]
42. Bashashati, A.; Fatourechi, M.; Ward, R.K.; E Birch, G. A survey of signal processing algorithms in brain–computer interfaces based on electrical brain signals. *J. Neural Eng.* **2007**, *4*, R32–R57. [CrossRef] [PubMed]
43. Lotte, F. Signal processing approaches to minimize or suppress calibration time in oscillatory activity-based brain–computer interfaces. *Proc. IEEE* **2015**, *103*, 871–890. [CrossRef]
44. Nicolas-Alonso, L.F.; Corralejo, R.; Gomez-Pilar, J.; Alvarez, D.; Hornero, R. Adaptive Stacked Generalization for Multiclass Motor Imagery-Based Brain Computer Interfaces. *IEEE Trans. Neural Syst. Rehabil. Eng.* **2015**, *23*, 702–712. [CrossRef] [PubMed]
45. Nourmohammadi, A.; Jafari, M.; Zander, T.O. A Survey on Unmanned Aerial Vehicle Remote Control Using Brain–Computer Interface. *IEEE Trans. Hum.-Mach. Syst.* **2018**, *48*, 337–348. [CrossRef]
46. Tam, W.-K.; Tong, K.-Y.; Meng, F.; Gao, S. A Minimal Set of Electrodes for Motor Imagery BCI to Control an Assistive Device in Chronic Stroke Subjects: A Multi-Session Study. *IEEE Trans. Neural Syst. Rehabil. Eng.* **2011**, *19*, 617–627. [CrossRef] [PubMed]
47. Lotte, F. A Tutorial on EEG Signal-processing Techniques for Mental-state Recognition in Brain–Computer Interfaces. In *Guide to Brain-Computer Music Interfacing*; Springer: London, UK, 2014; pp. 133–161.
48. Speier, W.; Deshpande, A.; Pouratian, N. A method for optimizing EEG electrode number and configuration for signal acquisition in P300 speller systems. *Clin. Neurophysiol.* **2015**, *126*, 1171–1177. [CrossRef] [PubMed]
49. Lindgren, J.T. As above, so below? Towards understanding inverse models in BCI. *J. Neural Eng.* **2017**, *15*, 012001. [CrossRef] [PubMed]
50. Suwannarat, A.; Pan-Ngum, S.; Israsena, P. Comparison of EEG measurement of upper limb movement in motor imagery training system. *Biomed. Eng. Online* **2018**, *17*, 103. [CrossRef]
51. Lo, C.-C.; Chien, T.-Y.; Chen, Y.-C.; Tsai, S.-H.; Fang, W.-C.; Lin, B.-S. A Wearable Channel Selection-Based Brain-Computer Interface for Motor Imagery Detection. *Sensors* **2016**, *16*, 213. [CrossRef]
52. McCrimmon, C.M.; Fu, J.L.; Wang, M.; Lopes, L.S.; Wang, P.T.; Karimi-Bidhendi, A.; Liu, C.Y.; Heydari, P.; Nenadic, Z.; Do, A.H. Performance Assessment of a Custom, Portable, and Low-Cost Brain-Computer Interface Platform. *IEEE Trans. Biomed. Eng.* **2017**, *64*, 2313–2320. [CrossRef]
53. Alotaiby, T.; El-Samie, F.E.A.; A Alshebeili, S.; Ahmad, I. A review of channel selection algorithms for EEG signal processing. *EURASIP J. Adv. Signal Process.* **2015**, *2015*, 66. [CrossRef]
54. Ang, K.K.; Guan, C.; Phua, K.S.; Wang, C.; Zhou, L.; Tang, K.Y.; Joseph, G.J.E.; Kuah, C.W.K.; Chua, K.S.G. Brain-computer interface-based robotic end effector system for wrist and hand rehabilitation: Results of a three-armed randomized controlled trial for chronic stroke. *Front. Neuroeng.* **2014**, *7*, 30. [CrossRef] [PubMed]
55. Ang, K.K.; Chua, K.S.G.; Phua, K.S.; Wang, C.; Chin, Z.Y.; Kuah, C.W.K.; Low, W.; Guan, C. A Randomized Controlled Trial of EEG-Based Motor Imagery Brain-Computer Interface Robotic Rehabilitation for Stroke. *Clin. EEG Neurosci.* **2015**, *46*, 310–320. [CrossRef] [PubMed]
56. Aghaei, A.S.; Mahanta, M.S.; Plataniotis, K.N. Separable Common Spatio-Spectral Patterns for Motor Imagery BCI Systems. *IEEE Trans. Biomed. Eng.* **2015**, *63*, 15–29. [CrossRef]
57. Chonnaparamutt, W.; Supsi, W. SEFRE: Semiexoskeleton Rehabilitation System. *Appl. Bionics Biomech.* **2016**, *2016*, 1–12. [CrossRef] [PubMed]
58. Schalk, G.; Mellinger, J. *A Practical Guide to Brain–Computer Interfacing with BCI2000: General-Purpose Software for Brain-Computer Interface Research, Data Acquisition, Stimulus Presentation, and Brain Monitoring*; Springer Science & Business Media: Berlin, Germany, 2010.
59. Kang, S.S.; Lano, T.J.; Sponheim, S.R. Distortions in EEG interregional phase synchrony by spherical spline interpolation: Causes and remedies. *Neuropsychiatr. Electrophysiol.* **2015**, *1*, 545. [CrossRef]
60. Delorme, A.; Makeig, S. EEGLAB: An open source toolbox for analysis of single-trial EEG dynamics including independent component analysis. *J. Neurosci. Methods* **2004**, *134*, 9–21. [CrossRef] [PubMed]
61. Lopez-Calderon, J.; Luck, S.J. ERPLAB: An open-source toolbox for the analysis of event-related potentials. *Front. Hum. Neurosci.* **2014**, *8*, 213. [CrossRef]
62. Bai, O.; Lin, P.; Vorbach, S.; Floeter, M.K.; Hattori, N.; Hallett, M. A high performance sensorimotor beta rhythm-based brain–computer interface associated with human natural motor behavior. *J. Neural Eng.* **2008**, *5*, 24–35. [CrossRef]
63. Ibáñez, J.; I Serrano, J.; Del Castillo, M.D.; Monge-Pereira, E.; Molina-Rueda, F.; Alguacil-Diego, I.; Pons, J.L. Detection of the onset of upper-limb movements based on the combined analysis of changes in the sensorimotor rhythms and slow cortical potentials. *J. Neural Eng.* **2014**, *11*, 056009. [CrossRef]
64. American Electroencephalographic Society. Guideline thirteen: Guidelines for standard electrode position nomenclature. *J. Clin. Neurophysiol.* **1994**, *11*, 111–113. [CrossRef]

65. Vidaurre, C.; Kawanabe, M.; von Bünau, P.; Blankertz, B.; Müller, K.R. Toward unsupervised adaptation of LDA for brain–computer interfaces. *IEEE Trans. Biomed. Eng.* **2010**, *58*, 587–597. [CrossRef]
66. Vidaurre, C.; Sannelli, C.; Müller, K.-R.; Blankertz, B. Machine-learning-based coadaptive calibration for brain-computer interfaces. *Neural Comput.* **2011**, *23*, 791–816. [CrossRef] [PubMed]
67. Sannelli, C.; Vidaurre, C.; Müller, K.-R.; Blankertz, B. Ensembles of adaptive spatial filters increase BCI performance: An online evaluation. *J. Neural Eng.* **2016**, *13*, 046003. [CrossRef] [PubMed]
68. De Boor, C.R. A Practical Guide to Spline. 1978. Available online: https://www.researchgate.net/publication/200744645 (accessed on 21 September 2022).
69. Perrin, F.; Pernier, J.; Bertrand, O.; Echallier, J. Spherical splines for scalp potential and current density mapping. *Electroencephalogr. Clin. Neurophysiol.* **1989**, *72*, 184–187. [CrossRef] [PubMed]
70. Carr, J. Neurological Rehabilitation, 2/e [Internet]. 2011. Available online: https://www.google.com/books?hl=en&lr=&id=LX94DDJhL4MC&oi=fnd&pg=PA79&dq=Neurological+Rehabilitation,+2/e.&ots=i19EtTkoOL&sig=wrrL_2_HIpL6cJwZvRP1seALPSY (accessed on 16 April 2020).
71. Tangermann, M.; Müller, K.-R.; Aertsen, A.; Birbaumer, N.; Braun, C.; Brunner, C.; Leeb, R.; Mehring, C.; Miller, K.J.; Müller-Putz, G.R.; et al. Review of the BCI competition IV. *Front. Neurosci.* **2012**, *6*, 55. [CrossRef] [PubMed]
72. Benjamin Blankertz. Data Set IVa for the BCI Competition III [Internet]. 2004. Available online: https://www.bbci.de/competition/iii/desc_IVa.html (accessed on 23 September 2022).
73. Li, J.; Zhang, L. Bilateral adaptation and neurofeedback for brain computer interface system. *J. Neurosci. Methods* **2010**, *193*, 373–379. [CrossRef] [PubMed]
74. Savić, A.M.; Lontis, E.R.; Mrachacz-Kersting, N.; Popović, M.B. Dynamics of movement-related cortical potentials and sensorimotor oscillations during palmar grasp movements. *Eur. J. Neurosci.* **2020**, *51*, 1962–1970. [CrossRef] [PubMed]
75. Babiloni, C.; Carducci, F.; Cincotti, F.; Rossini, P.M.; Neuper, C.; Pfurtscheller, G.; Babiloni, F. Human movement-related potentials vs desynchronization of EEG alpha rhythm: A high-resolution EEG study. *Neuroimage* **1999**, *10*, 658–665. [CrossRef] [PubMed]
76. Iturrate, I.; Chavarriaga, R.; Pereira, M.; Zhang, H.; Corbet, T.; Leeb, R.; Millán, J.d.R. Human EEG reveals distinct neural correlates of power and precision grasping types. *NeuroImage* **2018**, *181*, 635–644. [CrossRef]
77. Bodda, S.; Diwakar, S. Exploring EEG spectral and temporal dynamics underlying a hand grasp movement. *PLoS ONE* **2022**, *17*, e0270366. [CrossRef]
78. Neuper, C.; Wörtz, M.; Pfurtscheller, G. ERD/ERS patterns reflecting sensorimotor activation and deactivation. *Prog Brain Res.* **2006**, *159*, 211–222. [CrossRef] [PubMed]
79. Shepard, D. A Two-Dimensional Interpolation Function for Irregularly-Spaced Data. In Proceedings of the 23rd ACM National Conference, Las Vegas, NV, USA, 27–29 August 1968; ACM Press: New York, NY, USA, 1968; pp. 517–524. [CrossRef]
80. Harder, R.L.; Desmarais, R.N. Interpolation using surface splines. *J. Aircr.* **1972**, *9*, 189–191. [CrossRef]
81. Costa, A.P.; Møller, J.S.; Iversen, H.K.; Puthusserypady, S. Adaptive CSP for user independence in MI-BCI paradigm for upper limb stroke rehabilitation. In Proceedings of the 2018 IEEE Global Conference on Signal and Information Processing (GlobalSIP), Anaheim, CA, USA, 26–29 November 2018; pp. 420–423.
82. Nunez, P.L.; Srinivasan, R. *Electric Fields of the Brain: The Neurophysics of EEG*; Oxford University Press: Oxford, MI, USA, 2006.
83. Boontanom, S.; Kitisomprayoonkul, W.; Israsena, P. Effects of transcranial direct current stimulation to mu rhythm in stroke patients: A randomized single-blind crossover study. Department of Rehabilitation Medicine, Chulalongkorn University: Bangkok, Thailand, *Unpublished manuscript*.
84. Buch, E.; Weber, C.; Cohen, L.G.; Braun, C.; Dimyan, M.A.; Ard, T.; Mellinger, J.; Caria, A.; Soekadar, S.; Fourkas, A.; et al. Think to move: A neuromagnetic brain-computer interface (BCI) system for chronic stroke. *Stroke* **2008**, *39*, 910–917. [CrossRef] [PubMed]
85. Jimenez, I.A.C.; Acevedo, J.S.G.; Olivetti, E.C.; Marcolin, F.; Ulrich, L.; Moos, S.; Vezzetti, E. User Engagement Comparison between Advergames and Traditional Advertising Using EEG: Does the User's Engagement Influence Purchase Intention? *Electronics* **2022**, *12*, 122. [CrossRef]
86. Lakshminarayanan, K.; Shah, R.; Daulat, S.R.; Moodley, V.; Yao, Y.; Sengupta, P.; Ramu, V.; Madathil, D. Evaluation of EEG Oscillatory Patterns and Classification of Compound Limb Tactile Imagery. *Brain Sci.* **2023**, *13*, 656. [CrossRef] [PubMed]
87. Alimardani, M.; Gherman, D.E. Individual differences in motor imagery bcis: A study of gender, mental states and mu suppression. In Proceedings of the 2022 10th International Winter Conference on Brain-Computer Interface (BCI), Gangwon-do, Republic of Korea, 21–23 February 2022; pp. 1–7.
88. Gomez-Pilar, J.; Corralejo, R.; Nicolas-Alonso, L.F.; Álvarez, D.; Hornero, R. Neurofeedback training with a motor imagery-based BCI: Neurocognitive improvements and EEG changes in the elderly. *Med. Biol. Eng. Comput.* **2016**, *54*, 1655–1666. [CrossRef] [PubMed]
89. Belkacem, A.N.; Jamil, N.; Palmer, J.A.; Ouhbi, S.; Chen, C. Brain computer interfaces for improving the quality of life of older adults and elderly patients. *Front. Neurosci.* **2020**, *14*, 692. [CrossRef] [PubMed]
90. Mesin, L.; Cipriani, G.E.; Amanzio, M. Electroencephalography-Based Brain–Machine Interfaces in Older Adults: A Literature Review. *Bioengineering* **2023**, *10*, 395. [CrossRef]
91. Edelman, B.J.; Baxter, B.; He, B. EEG Source Imaging Enhances the Decoding of Complex Right-Hand Motor Imagery Tasks. *IEEE Trans. Biomed. Eng.* **2016**, *63*, 4–14. [CrossRef]

92. Mammone, N.; Ieracitano, C.; Morabito, F.C. A deep CNN approach to decode motor preparation of upper limbs from time–frequency maps of EEG signals at source level. *Neural Netw.* **2020**, *124*, 357–372. [CrossRef] [PubMed]
93. Seo, N.J.; Lakshminarayanan, K.; Lauer, A.W.; Ramakrishnan, V.; Schmit, B.D.; Hanlon, C.A.; George, M.S.; Bonilha, L.; Downey, R.J.; DeVries, W.; et al. Use of imperceptible wrist vibration to modulate sensorimotor cortical activity. *Exp. Brain Res.* **2019**, *237*, 805–816. [CrossRef] [PubMed]
94. Lakshminarayanan, K.; Shah, R.; Yao, Y.; Madathil, D. The effects of subthreshold vibratory noise on cortical activity during motor imagery. *Mot. Control.* **2023**, *27*, 559–572. [CrossRef] [PubMed]
95. Ju, Z.; Gun, L.; Hussain, A.; Mahmud, M.; Ieracitano, C. A Novel Approach to Shadow Boundary Detection Based on an Adaptive Direction-Tracking Filter for Brain-Machine Interface Applications. *Appl. Sci.* **2020**, *10*, 6761. [CrossRef]
96. Emsley, M.W.; Lowe, D.J.; Duff, A.R.; Harding, A.; Hickson, A. Data modelling and the application of a neural network approach to the prediction of total construction costs. *Constr. Manag. Econ.* **2002**, *20*, 465–472. [CrossRef]
97. Bodner, K.; Fortin, M.J.; Molnár, P.K. Making predictive modelling ART: Accurate, reliable, and transparent. *Ecosphere* **2020**, *11*, e03160. [CrossRef]
98. Aliakbaryhosseinabadi, S.; Dosen, S.; Savic, A.M.; Blicher, J.; Farina, D.; Mrachacz-Kersting, N. Participant-specific classifier tuning increases the performance of hand movement detection from EEG in patients with amyotrophic lateral sclerosis. *J. Neural Eng.* **2021**, *18*, 056023. [CrossRef]

Disclaimer/Publisher's Note: The statements, opinions and data contained in all publications are solely those of the individual author(s) and contributor(s) and not of MDPI and/or the editor(s). MDPI and/or the editor(s) disclaim responsibility for any injury to people or property resulting from any ideas, methods, instructions or products referred to in the content.